Self-diffusion of Sn atoms in Cu_3Sn probed by quasielastic nuclear resonant scattering of synchrotron radiation

H. Thiess,[1] A. Baron,[1] D. Ishikawa,[2] T. Ishikawa,[1,2] D. Miwa,[2] B. Sepiol,[3] and S. Tsutsui[1]
[1]*Spring-8/JASRI, 1-1-1 Kouto, Mikazuki-cho, Sayo-gun, Hyogo-ken 679-5198 Japan*
[2]*Spring-8/RIKEN, 1-1-1 Kouto, Mikazuki-cho, Sayo-gun, Hyogo-ken 679-5198 Japan*
[3]*Institut f. Materialphysik der Universität Wien, Strudlhofgasse 4, A-1090 Wien, Austria*
(Received 19 June 2002; revised manuscript received 19 September 2002; published 8 May 2003)

We report on studies to determine the elementary diffusion jump of minority Sn atoms in the γ phase of the intermetallic copper-tin alloy. The diffusionally accelerated decay from a crystalline $Cu_{84}Sn_{16}$ sample at elevated temperatures has been probed by quasielastic nuclear scattering of synchrotron radiation. The diffusional acceleration of the nuclear decay after excitation by a synchrotron flash shows a clear dependence on the sample orientation. Comparing this dependence to model calculations for the diffusionally accelerated decay suggests that tin jumps via antistructure sites of the $D0_3$ ordered crystal lattice.

DOI: 10.1103/PhysRevB.67.184302 PACS number(s): 66.30.−h, 76.80.+y

I. INTRODUCTION

A knowledge of the diffusion mechanism is a key for understanding the high temperature behavior of solids. In ordered structures, to preserve ordering, diffusion must take place by some special mechanism.

Radio-tracer diffusion studies on several intermetallic compounds have been carried out (see Ref. 1 for an overview). Arita *et al.*[2] investigated tin diffusion in the copper-tin β and γ phases, and they found a very fast tin diffusion of 1.3×10^{-12} $m^2\,s^{-1}$ at 848 K. Whereas the tracer method gives excellent results over an extended range for the diffusion constant, it is a macroscopic method and no direct conclusions about the underlying jump mechanisms can be drawn. In contrast to this macroscopic technique there exist several scattering methods which can reveal the elementary diffusion jump mechanism: Quasielastic neutron scattering (QNS), quasielastic Mößbauer scattering (QMS), and the most recent nuclear resonant scattering of synchrotron radiation (NRS) method.

The latter comes with some definite advantages regarding the probe properties: the small beam size and negligible divergence combined with high intensity relative to QMS make it the method of choice when using small or inhomogeneous samples. So far diffusion studies with NRS on single crystals have been exclusively applied to compounds containing the ^{57}Fe isotope: FeAl and most extensively Fe_3Si.[3,4] For Fe_3Si, QMS and NRS have proven that the majority component iron, which occupies sites on three sublattices, jumps between nearest neighbor iron sites on different sublattices, remaining on each sublattice for different residence times.

In this paper we present measurements of the diffusion of tin atoms in an off-stoichiometric copper-tin sample with two significant differences from previous work: Diffusion measurements with NRS from tin nuclei have been performed for the first time, to our knowledge. It appears a challenge to extend diffusion investigations with the NRS method to another important Mößbauer isotope, and to check the underlying jump model for the *minority* component in the $D0_3$ structure which is still in question.[5]

II. DIFFUSION IN THE γ PHASE OF CU SN ALLOYS

Copper-tin alloys have been used since ancient times. At present they attract much interest since the growth of copper-tin intermetallic compounds plays an important role in the kinetics of the soldering reaction, used in microelectronics packaging (see, for example, Ref. 6). Therefore it is no wonder that various studies have been reported on their phase diagram and diffusion behavior. A very interesting phase for diffusion investigations is the so called γ phase in the copper-tin system.[2,7] This high temperature phase which has a $D0_3$ structure crystallizes at tin concentrations between 14.9 and 28 at. %. For the stoichiometric composition Cu_3Sn the alloy crystallizes in the $D0_3$ phase only in a narrow temperature range of approximately 30 K. Therefore diffusion experiments have usually been performed with off-stoichiometric samples. At a tin concentration of 17% the γ phase extends from 793 to 1028 K, which marks the lowest stable temperature for this phase.[8]

A schematic representation of the $D0_3$ structure is given in Fig. 1. This structure can be decomposed into three sublattices, a simple cubic sublattice α which accommodates 50% of the atoms and two interpenetrating face centered cubic lattices γ and β, where each fcc sublattice contains 25% of the atoms. At stoichiometric composition A_3B the A atoms occupy the α and γ sublattices and the B atoms the β sublattice. In the case of $A_{83}B_{17}$ about 1/3 of the B atoms on the β sublattice will be statistically replaced by A atoms. This arrangement implies a fundamental difference for the self diffusion of A and B atoms in a $D0_3$ phase: A atoms can migrate via simple nearest neighbor jumps within sublattices occupied by the same species, whereas all nearest neighbor sites of the B atoms are sites occupied by A atoms. For B atoms to reach the closest β site occupied with their own species would require a next next nearest neighbor jump, which is unlikely. This implies the migration via antistructure sites on the α and γ sublattices.

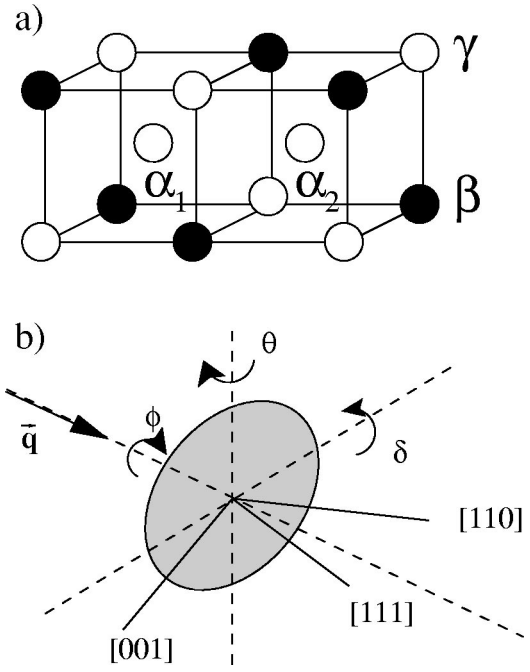

FIG. 1. (a) Simple sketch of the $D0_3$ structure. 1/4 of the elementary cell is shown. At stoichiometry the β site is occupied with the minority component tin (filled circles) and all other sublattices with the majority component copper. (b) Orientation of the sample in the beam. For $\theta = 0°$ the wave vector $\vec{q}$ points about 8° from the [111] crystal axis toward the [110] axis. Changing θ means moving the wave vector $\vec{q}$ in the [001],[110] plane. The angles φ and δ are defined to account for an initial disorientation of the crystal.

In order to transform these considerations into a formalism that can be used later to draw conclusions from the diffusion data obtained by NRS we use the jump matrix **A** (see Ref. 9,10 for details). **A** conducts the rate equation for the intermediate scattering function $I(\vec{q},t)$ through $(\partial/\partial t)I(\vec{q},t) = \mathbf{A}I(\vec{q},t)$. Its elements specify the various allowed jumps for the diffusing tin atoms and the related jump rates:

$$A_{ij}(\vec{q}) = \sqrt{\frac{c_j}{c_i}}\left[-\frac{1}{n_{ji}\tau_{ji}}\sum_k \exp(-\imath\,\vec{q}\cdot\vec{l}_{ij}^{\,k}) - \delta_{ij}\sum_l \frac{1}{\tau_{il}}\right]. \tag{1}$$

Here each site of the ith sublattice is surrounded by n_{ij} sites of the jth sublattice with the kth site located at the vector distance $\vec{l}_{ij}^{\,k}$. $1/\tau_{ji}$ is defined as the jump rate from a site of symmetry i to a neighbor site of symmetry j. c_i is the probability for the occupation of the ith sublattice by a tin atom. The jump matrices for the different possible jumps of the tin atoms within the $D0_3$ structure of the copper-tin γ phase can be calculated, according to Eq. (1). In the case of $\beta\alpha$ jumps the α sublattice is, for simplicity, subdivided into two sublattices α_1 and α_2, where each sublattice taking 25% of the atoms (also see Fig. 1). However, since both α sublattices look the same for the diffusing atoms they are characterized by the same concentration and residence time. In a first approach we confine ourself to $\beta\alpha$ nearest neighbor jumps, neglecting $\alpha\gamma$ jumps. Then the result is a 3×3 dimensional jump matrix for $\beta\alpha$ jumps of the following form:

$$\mathbf{A}_{\beta\alpha}(\vec{q}) = \begin{pmatrix} -\frac{2}{\tau_{\beta\alpha}} & \sqrt{\frac{c_\alpha}{c_\beta}}\frac{1}{\tau\alpha\beta}E & \sqrt{\frac{c_\alpha}{c_\beta}}\frac{1}{\tau\alpha\beta}E^* \\ \sqrt{\frac{c_\beta}{c_\alpha}}\frac{1}{\tau\beta\alpha}E^* & -\frac{1}{\tau_{\alpha\beta}} & 0 \\ \sqrt{\frac{c_\beta}{c_\alpha}}\frac{1}{\tau\beta\alpha}E & 0 & -\frac{1}{\tau_{\alpha\beta}} \end{pmatrix}, \tag{2}$$

where E is a complex function of the lattice structure, $E = \cos(q_x a/4)\cos(q_y a/4)\cos(q_z a/4) + \imath\sin(q_x a/4)\sin(q_x a/4)\sin(q_x a/4)$, $1/\tau_{\beta\alpha}$, and $1/\tau_{\alpha\beta}$ are the jump rates from β to α sites, and vice versa. q_x, q_y and q_z are the cartesian components of the radiation wave vector $\vec{q}$. For $\beta\gamma$ a simple 2×2 dimensional jump matrix and for $\beta\beta$ jumps a simple scalar suffice. An analogous notation to Eq. (2) yields

$$\mathbf{A}_{\beta\gamma}(\vec{q}) = \begin{pmatrix} -\frac{1}{\tau_{\beta\gamma}} & \sqrt{\frac{c_\gamma}{c_\beta}}\frac{E_\gamma}{\tau_{\gamma\beta}} \\ \sqrt{\frac{c_\beta}{c_\gamma}}\frac{E_\gamma}{\tau_{\beta\gamma}} & -\frac{1}{\tau_{\gamma\beta}} \end{pmatrix}. \tag{3}$$

The function of the lattice structure is $E_\gamma = 2[\cos(q_x a/2) + \cos(q_y a/2) + \cos(q_z a/2)]$. For $\beta\beta$ jumps the jump matrix becomes a scalar with $E_\beta = \cos[(q_x - q_y)a/2] + \cos[(q_x + q_y)a/2] + \cos[(q_x - q_z)a/2] + \cos[(q_y + q_z)a/2]$. The jump matrix associates the phase shift caused by the atomic motion along every possible jump vector $\vec{l}$. This phase shift is expressed through the projection of the outgoing wave vector $\vec{q}$ onto the jump vectors.

III. PRINCIPLES OF DIFFUSION MEASUREMENTS WITH NRS

NRS enables studies in the time domain. The general idea using NRS is that the state which forms due to the directed and pulsed excitation of resonant nuclei is disrupted by diffusion. When the time between diffusive jumps becomes comparable or even shorter than the natural lifetime of the diffusing nucleus ($\tau_0 = 25.6$ ns), diffusion leads to a faster decay of the scattered intensity in forward direction with respect to the undisturbed process. From this ''diffusionally accelerated'' decay, details on the diffusion process can be derived. NRS into the forward direction is often denoted as *nuclear forward scattering* (NFS).

The intensity of the forward scattered radiation I_{NFS}, as a function of the sample thickness z and time after excitation t, can be expressed by the following relation:[11]

$$I_{NFS}(t,z)=I_0(z)\left|\int_{-\infty}^{+\infty}\frac{d\omega}{2\pi}\exp(-\imath\omega t)\times\exp\left(-\frac{1}{2}L(z)\varphi(\vec{q},\omega)\right)\right|^2, \quad (4)$$

where ω is the energy deviation from exact resonance, $\varphi(\vec{q},\omega)$ is the *universal resonance function*,[12] $L(z)=\sigma_0 f_{LM} n\chi z$ the samples effective thickness with σ_0 the nuclear absorption cross section at the ^{119}Sn resonance, f_{LM} is the Lamb-Mößbauer factor, n is the number of tin atoms per unit volume, and χ is the ^{119}Sn isotope abundance. $I_0(z)$ is the incoming intensity within the frequency band that is transmitted by the monochromator system reduced by the electronic absorption in the sample. The universal resonance function $\varphi(\vec{q},\omega)$ (Ref. 12) contains all dynamical effects on NRS spectra. Note that this function is of very general validity as the same function can be used to mirror dynamical effects in QNS and QMS. For diffusion on non-Bravais lattices $\varphi(\vec{q},\omega)$ is in general a superposition of Lorentzian shaped lines with different weights and linewidths:

$$\varphi(\vec{q},\omega)=\imath\sum_p \frac{w_p(\vec{q})\Gamma_0/2\hbar}{\omega+i(\Gamma_0-\Gamma_p(\vec{q}))/2\hbar}. \quad (5)$$

Γ_0 is the natural energy width of the nuclear transition of the tin nuclei, $w_p(\vec{q})$ is the weight for each line and $\Gamma_p(\vec{q})$ denotes the energetically broadening of Lorentzian shaped lines caused by diffusion, the *diffusional line broadening*. The width and broadening can be calculated from the jump matrix **A** from Eqs. (2) and (3), respectively, $-\Gamma_p(\vec{q})/2\hbar$ is the pth *eigenvalue* of matrix **A** and $w_p(\vec{q})=|\Sigma_i\sqrt{c_i}b_i^p|^2$, where the b_i^p is the ith component of the pth *eigenvector* of **A**. We note that *diffusional line broadening* in the energy domain corresponds to the *diffusionally accelerated decay* in the time domain. Since it is very convenient to discuss diffusion with the help of $\varphi(\vec{q},\omega)$, but experimental data are described by $I_{NFS}(t,z)$ in Eq. (4), we will use both terms as aliases for one and the same thing: The effect of diffusion to scattering methods.

From Eq. (5), where Γ_p and w_p result from the eigenvalues and eigenvectors of the jump matrix in Eqs. (2) and (3), respectively, the orientation dependence of the diffusional line broadening can be calculated. Meanwhile the values for Γ_p and w_p can be extracted from the experimental data by fits to the time spectra according to Eq. (4). The present work studies the underlying jump mechanism by comparing the experimental data with calculations for the possible nearest neighbor and next nearest neighbor jumps of tin atoms in the $D0_3$ lattice.

IV. EXPERIMENT

The sample was prepared by resistivity melting under argon atmosphere of the pure elements copper and tin. The tin was isotopically enriched to 80% ^{119}Sn. The specimen were weighted to give a tin concentration of 17 at. %. Our $Cu_{0.83}Sn_{0.17}$ sample has been remelted several times, and an oval slice has been cut from the center of the sample. The transverse samples dimensions are 4.5×3.5 mm^2, with thicknesses of approximately 145 and 165 μm, respectively. The slice has been heated for 48 h at 1000 K under an argon atmosphere for recrystallization in the high temperature γ phase just below the phase transition into the liquid state. In order to preserve the metastable γ phase the sample was subsequently quenched to room temperature. A systematic study with Laue photographs has been performed to check the orientation of the annealed sample. Within 3 mm around the samples center a cubic structure could be identified by finding the symmetry pattern which correspond to the [111] and [110] directions, respectively. No additional pattern could be identified within this area. To check that the metastable phase was preserved after the heating and cooling procedure in the experiment, Laue patterns were taken before and after the experiment and they show good agreement.

Measurements have been carried out at the x-ray undulator beamline BL35XU, at SPring-8.[13] During the measurements the sample was kept inside a vacuum furnace in order to adjust the measuring temperatures between room temperature and 946 K while the sample was kept in vacuum. The sample was mounted between two thin BeO disks filled with Al_2O_3 powder. The orientation of the sample was such that the plane spanned by the lattice vectors [001] and [110] was horizontal. An evaluation of the Laue patterns and additional diffractometer measurements show that the surface normal was 8° from the [111] direction toward [110] (see Fig. 1). We note that the diffractometer measurements show strongly broadened nonsymmetric Bragg reflections. The width is several mrad, approximately 100 times the typical width of the rocking curve, which indicates that the sample exibits a pronounced mosaic structure rather than a single crystalline structure. In the forward scattering setup the sample mounting permits changes of the sample orientation relative to the incoming synchrotron beam of about $\pm20°$. The furnace was mounted on a diffractometer to facilitate the rotation of the sample relative to the beam.

The storage ring was operated in timing mode providing x-ray pulses of very short duration [less than 70-ps full width at half maximum (FWHM)] with a repetition time of 57 ns. This time structure matches well the lifetime of the nuclear decay of the ^{119}Sn resonance of 25.6 ns. The synchrotron radiation generated by an in-vacuum undulator was monochromatized by a two-stage monochromator setup to a final bandwidth of $\approx$1.4 meV.[14] The size of the beam spot at the sample position was about 1.5×0.5 mm^2 (horizontal $\times$ vertical). Forward scattered photons were detected by an linear array of 16 avalanche photo diodes operated in grazing incidence geometry. This array combines excellent time resolution of $\approx$ 180 ps FWHM with 25% efficiency at the 23.9 keV resonance of ^{119}Sn.[15] Discrimination and a fast electronic gating of the detector signal permitted measurements of the delayed signal starting from 5 ns after the radiation flash. The typical count rate was between 1 and 4 Hz.

Two sets of measurements have been carried out. For the first dataset the sample was heated to 828 K, and time spectra were recorded at eight different orientations of the sample relative to the synchrotron beam. Hereby the sample was

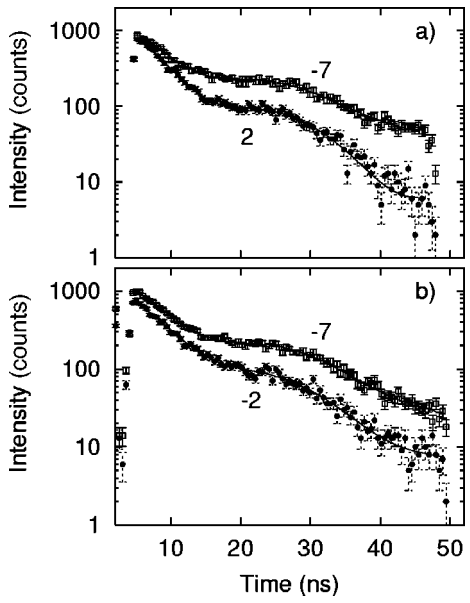

FIG. 2. Time spectra of nuclear forward scattering: Two representative spectra from the first (a) and second (b) datasets are shown together with their fits (solid lines). In (a) the open squares correspond to the spectrum taken at $\theta = -7°$ and the circles at 2°. In (b) the the symbols represent spectra taken at $-7°$ and $-2°$, respectively. One can easily note the change in the diffusional acceleration with the orientation and the beating structure due to an additional contribution, identified as an SO_2 layer.

rotated around the vertical axis in an angular range from -7 to 27° between the samples [111] direction and the synchrotron beam. The second set of data was taken at 838 K. The sample was again rotated around the vertical axis, and

TABLE I. Results for the fits to the time spectra data listed in the order of their measurement. For each orientation the diffusional line broadening $\Delta\Gamma_{narrow}$ of the narrow line and the weight of the broad line weight$_{broad}$ have been fitted. The width of the broad line and the values for the additional third site were held fixed. The angle θ is the angle between the [111] direction and the radiation wave vector, when turning around the vertical axis toward the [110] direction.

θ (°)	$\Delta\Gamma_{narrow}$ (Γ_0)	Weight$_{broad}$
8	1.53(14)	0.14(11)
10	1.31(7)	0.08(6)
14	1.44(5)	0.01(5)
18	1.24(5)	0.22(3)
22	1.37(8)	0.19(5)
27	1.67(9)	0.20(5)
-7	0.09(3)	0.20(3)
2	1.67(8)	0.05(6)
3	1.40(7)	0.05(6)
-2	1.46(7)	0.01(6)
-7	0.35(3)	0.20(3)
8	1.33(4)	0.01(5)
-12	1.18(6)	0.26(4)
-9	0.68(4)	0.01(4)

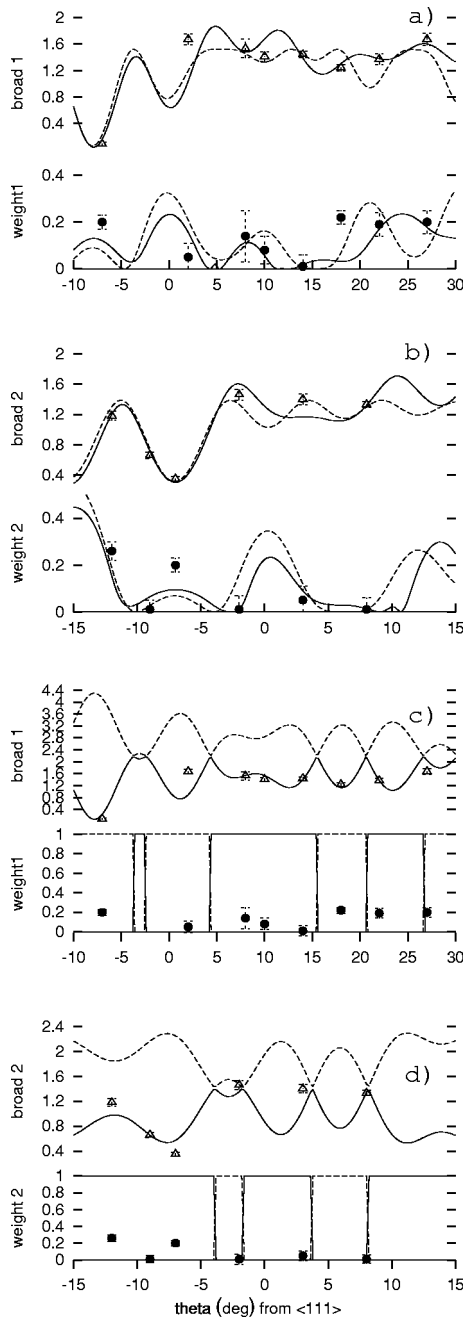

FIG. 3. Orientation dependence of the diffusion effect for datasets 1 (a) and 2 (b). The data points represent the results for the weight of the broad line (weight) and the diffusional broadening of the narrow line (broad) from the fits to the time spectra (see Table I). The solid line represents the best fit for the $\beta\alpha$ jumps model whereas the dashed line stands for the best fit with the $\beta\gamma$ model (Table II). The difference in the best fits between the models does not allow to exclude one model. (c) and (d) show the old and new datasets resp. together with the best fits according to the model of $\beta\beta$ jumps. The weight of the two components shows an alternating behavior. The result can be understood as one single broadened line with a constant weight of unity. The best fit has been obtained by using only the component represented by the solid line. The best fit for the $\beta\beta$ jump model clearly disagrees with the measured data. Using both components fits the data even less.

time spectra obtained at six different orientations ($-12°$ to $8°$). Before and after the high temperature measurements time spectra have been recorded at low temperatures (423 and 623 K). The thickness of the sample in the first dataset was 165 ± 10 μm. For the second dataset the sample was polished down to 145 ± 10 μm.

V. RESULTS

Characteristic time spectra taken at different orientations from each dataset are shown in Fig. 2. Already at first glance one can identify two main characteristics of the spectra: They exhibit a rather smooth beating structure with a bump at about 25 ns and a rather strong dependence of the slope of the intensity decay on the sample orientation. Examination shows that the fraction of the beating structure to the intensity grew after heating the sample in the beginning of the experiment and then quickly saturated.

For fitting the NFS time spectra with the MOTIF program[16] three different nuclear sites have been included: Sites 1 and 2 account for the presence of a narrow and a strongly diffusionally broadened line. In the fits the sum of their weights was held constant. The third site accounts for the additional beating structure. This selection accommodates the idea that a tin compound other than the copper-tin compound is formed during heating, probably caused by bad vacuum conditions inside the furnace. Simulations of time spectra at high temperatures show that a low fraction component (13% of the effective thickness at saturation) with an isomer shift of $5.5\Gamma_0$ averaged over $1.7\Gamma_0$ accounts very well for the observed beating structure. It is important to note that the third spectral component, that shows a strong presence in the high temperature spectra, in fact corresponds to a very low contamination. This is since the effective thickness of the Cu-Sn compound shows a huge drop when entering the γ phase, whereas the effective thickness of the third spectral component stays almost constant. From NFS time spectra taken at low temperatures we could estimate the contamination to be less then 1 at %. Comparison with literature[17] yields very good agreement with values found for SnO_2. Therefore we assume that SnO_2 formed on the sample surface after sample heating.

Limited statistics in the time spectra makes it necessary to strictly limit the number of fitted parameters. Therefore data from both datasets have been fitted in a uniform manner: the isomer shift and weight for the third site were held fixed. A simulation of the spectra showed the best agreement when choosing a diffusional line broadening of about $5\Gamma_0$ for the strongly broadened line. The relative weight of line 1 with respect to line 2 and the diffusional broadening of line 2 have been fitted. Results of the fits are summarized in Table I. The dependence of the line broadening on the sample orientation is shown in Fig. 3. The line broadening in our time spectra is governed by the contributions from the narrow line with high weight and a strongly broadened line with a considerably lower weight. We note that this points to the case where tin-atom occupy different lattice sites with considerably different residence times on each sublattice.

To learn about the diffusion mechanism from the orientation dependence of the diffusional line broadening we compare the line broadening and relative weight between the lines obtained from the fits to the data with the calculations according to the various jump models presented in Sec. II. Since a detailed comparison of all individual lines is beyond the scope of the statistics in our spectra, we compare the characteristics of the orientation dependence of the diffusional line broadening and the relative weights between one narrow line and one broadened line since these values show a significant orientation dependence. By this procedure we want to determine the jump model whose broadening characteristics suit our data best.

The CERN-Minuit package[18] was used to simultaneously fit $\Delta\Gamma_{narrow}(\vec{q})$ and w_{broad} to all three jump models presented in Sec. II and the two datasets successively. The initial sample orientation and the relative residence times for different sublattices occupied by tin atoms and the jump rates τ^{-1} between the site on neighboring sublattices have been freely adjusted. Figure 3 shows the results for the best fits for all three jump models. Table II gives the corresponding sets of fit parameters together with the χ^2 values for the best fit.

The orientation of the sample has been determined before the experiment by an evaluation of the sample Laue patterns. However, the mounting of the sample definitely results in the loss of exact knowledge of the orientation during the experiment. The possible disorientation of several degrees for the ϕ angle and $1°-3°$ for θ and δ have not been recognized as crucial before this experiment, to our knowledge. However,

TABLE II. Results from the comparison of the orientation dependence of the broadening of the narrow line and the weight of the broad line. The jump rate τ^{-1} and the percentage of tin atoms on the beta site follow directly as parameters from the fit. *R* represents the reduced χ^2 value of the fit.

Jumps	$\beta\alpha$		$\beta\gamma$		$\beta\beta$	
Dataset	1	2	1	2	1	2
τ^{-1}	1.69(4)	1.43(4)	2.66(6)	2.32(6)	4.37(9)	2.82(8)
c_β (%)	82(2)	72(6)	87(1)	84(1)	-	-
ϕ (°)	5.9(5)	9.5(8)	7.8(5)	9.9(9)	5.9(4)	0.6(10)
δ (°)	1.9(1)	4.2(2)	2.6(1)	4.2(2)	1.9(4)	3.5(4)
θ_0 (°)	$-0.1(1)$	$-0.9(1)$	0.1(1)	$-0.7(1)$	$-0.21(6)$	$-3.85(18)$
R	8.5	5.2	10.4	5.6	16.7	14.6

the large wave vector for ^{119}Sn compared to the ^{57}Fe resonance make the orientation dependence of the diffusional acceleration change with much smaller disorientations. This makes the determination of the exact sample orientation a severe requirement.

Since the furnace was mounted on a diffractometer, the relative rotation of the sample is determined very precisely. In the evaluation we account for this uncertainty by a free fit of the samples orientation while taking the relative orientation difference due to the rotation around the vertical axis as a fixed parameter.

The model for $\beta\beta$ jumps clearly disagrees with the collected data, indicating that tin atoms migrate via antistructure sites. This leaves the possibility of $\beta\alpha$ jumps and $\beta\gamma$ jumps for the tin atoms. The result from our evaluation indicates that the model corresponding to $\beta\alpha$ jumps fits a little better to the measured data than $\beta\gamma$ jumps but we feel that this difference is not significant enough to privilege one mechanism over the other. For the discrimination between $\beta\gamma$ and $\beta\alpha$ jumps via antistructure sites additional NFS time spectra taken at additional θ values would be of great value. Figure 4 shows a simulation of the weight of the strongly broadened line at θ values around $-25°$, which roughly corresponds to the [113] crystal axis. At these orientations both models predict strong discrepancies for the weight of the broad line and therefore would allow to decide about the antistructure site via which the tin atoms migrate.

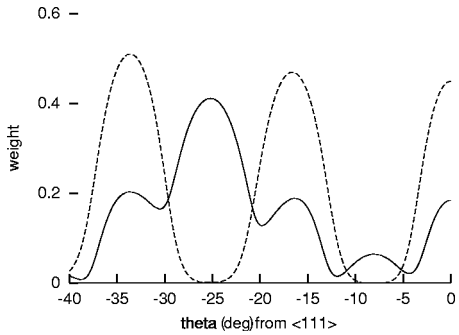

FIG. 4. Simulation of the weight of the strongly broadened line when changing the θ angle around the crystal [113] direction. For the simulations 80% of the tin atoms are assumed to be located on the β sublattice, which matches the results from the present measurements. The solid line corresponds to $\beta\alpha$ jumps whereas the broken line stands for $\beta\gamma$ jumps. Around the [113] direction $(-25°)$ the simulations for the weight of the broad line predicts strong discrepancies between the models.

VI. CONCLUSION

In conclusion we demonstrate that it is possible to investigate diffusion by observing the diffusionally accelerated decay from ^{119}Sn nuclei when scattered from a $Cu_{83}Sn_{17}$ sample. The diffusional acceleration exhibits a pronounced orientation dependence. An analysis of the this orientation dependence has been performed by a comparison with simulations for neighbor jumps within the $D0_3$ structure of the Cu-Sn sample. To our knowledge, this is the first direct observation of the atomistic diffusion mechanism in the copper tin compound. The comparison indicates that Sn atoms migrate via jumps on antistructure sites on the copper sublattice. However the collected data does not allow one to select if the migration takes place via $\beta\alpha$ jumps or $\beta\gamma$ jumps or even a mixture of those. In order to decide on the antistructre sites via which the tin atoms migrate, measurements might be carried out with a careful orientation of the mounted sample in the beam and with the wave vector around the [113] axis of the crystal. Furthermore a pronounced asymmetry of the jump frequencies between $\beta\alpha$ and $\alpha\beta$ jumps indicates a concentration difference of tin atoms in favor of the β site.

ACKNOWLEDGMENTS

H.T. wants to thank A. Barla for discussions and for encouragement with the tin measurements. He acknowledges the financial support from JSPS fellowship No. PB01719.

[1] H. Mehrer, Mater. Trans., JIM **37**, 1259 (1996).
[2] M. Arita, H. Nakajima, M. Koiwa, and S. Miura, Mater. Trans., JIM **32**, 32 (1991).
[3] B. Sepiol, A. Meyer, G. Vogl, R. Rüffer, A. I. Chumakov, and A. Q. R. Baron, Phys. Rev. Lett. **76**, 3220 (1996).
[4] B. Sepiol, A. Meyer, G. Vogl, H. Franz, and R. Rüffer, Phys. Rev. B **57**, 10433 (1998).
[5] I. V. Belova and G. E. Murch, J. Phys. Chem. Solids **59**, 1 (1998).
[6] H. K. Kim and K. N. Tu, Phys. Rev. B **53**, 16027 (1996).
[7] N. Prinz and H. Wever, Phys. Status Solidi A **61**, 505 (1980).
[8] M. Hansen, *Constitution of Binary Alloys* (McGraw-Hill, New York, 1958).
[9] B. Sepiol and G. Vogl, Phys. Rev. Lett. **71**, 731 (1993).
[10] O. G. Randl, B. Sepiol, G. Vogl, R. Feldwisch, and K. Schroeder, Phys. Rev. B **49**, 8768 (1994).
[11] V. G. Kohn and G. V. Smirnov, Phys. Rev. B **57**, 5788 (1998).
[12] In Ref. 11 Kohn and Smirnov denote φ the *universal resonance function*, a name that shall be used in the present publications as well. We note that in other publication dealing with diffusion measurements with scattering methods, especially in those refering to QNS, φ is named the *momentum-energy correlation function*.
[13] A. Baron, Y. Tanaka, S. Goto, K. Takeshita, M. Matsushita, and T. Ishikawa, J. Phys. Chem. Solids **61**, 461 (2000).
[14] D. Miwa and D. Ishikawa, work in progress, design based on A. Baron, Y. Tanaka, D. Ishikawa, D. Miwa, M. Yabashi, and T. Ishikawa, J. Synchrotron Radiat. **8**, 1127 (2001).
[15] A. Q. R. Baron (unpublished).
[16] Y. Shvyd'ko, *MOTIF, A program for Mößbauer time spectra of nuclear forward scattering, Users Guide* (1998).
[17] R. C. Reno, M. J. Panunto, and B. H. Piekarski, J. Electron. Mater. **26**, 11 (1997).
[18] *CN/ASD Group, MINUIT – Users Guide, Program Library D506. CERN* (1993).